forests

MDPI

Article

Alternative First Exons Drive Enzymatic Activity Variation in Chalcone Synthase 3 of *Dendrobium sinense*

Yu Wang [1,†], Liyan Liu [1,†], Qiongjian Ou [1], Huiyan You [1], Jia Wang [1,2,*] and Jun Niu [1,2,*]

[1] Key Laboratory of Genetics and Germplasm Innovation of Tropical Special Forest Trees and Ornamental Plants, School of Tropical Agriculture and Forestry, Hainan University, Haikou 570228, China
[2] Collaborative Innovation Center of Ecological Civilization, Hainan University, Haikou 570228, China
* Correspondence: wangjia9201@hainanu.edu.cn (J.W.); niujun@hainanu.edu.cn (J.N.)
† These authors contributed equally to this work.

Abstract: *Dendrobium sinense*, a native orchid species of Hainan Island, is cultivated for its ornamental flowers. Recently, this species has gained significant attention due to its medicinal value. This study focuses on the identification of type III polyketide synthase (PKS), which catalyzes the formation of crucial intermediates in secondary metabolites. Through analysis of previous transcriptome data, a total of ten type III *DsPKS* genes were identified. Phylogenetic analysis categorized the type III PKS proteins into CHS, BBS, and PKS groups. Interestingly, the *DsCHS3* gene exhibited alternative first exons, resulting in two splice variants, namely *DsCHS3-1* and *DsCHS3-2*. Full-length cDNA sequencing revealed that *DsCHS3-1* was the more prevalent splice variant. Prokaryotic expression and purification of DsCHS3-1 and DsCHS3-2 proteins were successfully achieved. Enzyme activity analysis demonstrated significantly higher catalytic activity in DsCHS3-2 compared to DsCHS3-1, particularly in the conversion of *p*-coumaryol-CoA and malonyl-CoA to naringin chalcone. Functional complementation assays in *Arabidopsis* mutants confirmed the higher catalytic activity of *DsCHS3-2*, as it restored flavonoid biosynthesis to a greater extent compared to *DsCHS3-1*. Overall, these findings offer valuable insights into the alternative splicing patterns and functional divergence of *DsCHS3* genes in *D. sinense*.

Keywords: *Dendrobium sinense*; type III polyketide synthase; alternative first exons; *DsCHS3*; protein activity; flavonoid biosynthesis

check for updates

Citation: Wang, Y.; Liu, L.; Ou, Q.; You, H.; Wang, J.; Niu, J. Alternative First Exons Drive Enzymatic Activity Variation in Chalcone Synthase 3 of *Dendrobium sinense*. *Forests* **2023**, *14*, 1702. https://doi.org/10.3390/f14091702

Academic Editor: Heinz Rennenberg

Received: 25 July 2023
Revised: 11 August 2023
Accepted: 18 August 2023
Published: 24 August 2023

Copyright: © 2023 by the authors. Licensee MDPI, Basel, Switzerland. This article is an open access article distributed under the terms and conditions of the Creative Commons Attribution (CC BY) license (https://creativecommons.org/licenses/by/4.0/).

1. Introduction

The Orchidaceae family encompasses a vast array of germplasm resources, comprising more than 28,000 distinct species, which are classified into over 800 genera across five subfamilies. These diverse species predominantly inhabit tropical and subtropical regions [1]. Some of the notable Orchidaceae species, including *Phalaenopsis*, *Dendrobium*, *Cymbidium*, *Bletilla*, and *Gastrodia* plants, are cultivated for their significant aesthetic, cultural, and pharmaceutical value. *Dendrobium*, the second-largest genus within the Orchidaceae family, typically thrives in warm, moist, and semi-shaded environments, often as epiphytes on tree trunks or rocks [2]. *Dendrobium* species have attracted significant attention due to their abundant reserves of polysaccharides, alkaloids, flavonoids, and other bioactive compounds [3]. These compounds have been widely utilized in healthcare due to their notable anti-aging, anti-oxidation, and anti-tumor properties [3,4].

Dendrobium sinense, a perennial epiphytic plant, is distributed in the mountainous areas of central and western Hainan Island, including the counties of Lingshui, Baoting, and Qiongzhong [5]. *D. sinense* stands out as a precious and endemic species on Hainan Island, holding significant economic value. Morphologically, its flowers are white, solitary, and located at the apex of the stem. With several petals, they collectively present an aesthetically pleasing appearance, adding to the plant's high ornamental value. Notably, *D. sinense*

has been extensively used as traditional ethnic medicine in Hainan [6]. This species exhibits remarkable capabilities in synthesizing various bioactive compounds, including alkaloids, bibenzyls, flavonoids, phenanthrenes, polysaccharides, and other valuable constituents [6–8]. Consequently, there has been an increasing interest in investigating the pharmacological effects and molecular mechanisms associated with *D. sinense.* For instance, four bibenzyls and twelve phenolic compounds were isolated from the entire *D. sinense* plant [9]. Furthermore, the characterization of a *bibenzyl synthase* (*BBS*) genes in *D. sinense* has yielded valuable insights into potential biosynthetic pathways [5]. Metabolomics in *D. sinense* unveiled a significant abundance of phenylpropanoids and polyketides, with many of these compounds responding to drought stress [10]. Despite progress, our understanding of the regulatory mechanisms underlying the active ingredients in this species remains limited.

Polyketides constitute a substantial class of secondary metabolites present in plants that fulfill crucial roles in biotic and abiotic stress responses, signaling pathways, and tissue compositions [11]. This category of natural compounds is widely recognized for its potential therapeutic applications, including antimicrobial, anticancer, antiparasitic, and anti-cholesterol properties [12]. The biosynthesis of polyketides is governed by a group of enzymes known as polyketide synthases (PKS), which facilitate the sequential condensation of simple two-carbon acetate units with an acyl starter molecule [13]. PKS is generally classified into three types based on protein domains and catalytic mechanisms [14]. Type I PKS is characterized by multiple catalytic modules and is primarily responsible for catalyzing the biosynthesis of compounds such as erythromycin, sirolimus, and rifamycin, typically found in fungal or bacterial systems [15]. Type II PKS, comprising two ketosynthase units (α- and β-ketosynthase), is specifically involved in the production of bacterial aromatic polyketides, such as anthracyclines and tetracyclic compounds [16]. Type III PKS features a relatively simpler structure but plays a significant role in generating a diverse array of polyketide compounds, such as chalcones, pyrones, acridones, phloroglucinols, stilbenes, and bibenzyls [12].

In plants, type III PKS emerges as a pivotal enzyme that partakes in the biosynthesis of secondary metabolites [11]. This enzyme family comprises a range of enzymes including chalcone synthase (CHS), stilbene synthase, acridone synthase, stilbenecarboxylate synthase, and BBS [15]. Notably, plant type III PKSs facilitate cyclization reactions of polyketides, which can be classified into three main types: Claisen cyclization, aldol cyclization, and lactonization [11]. According to our previous next-generation sequencing analysis, the CHS type predominantly prevails within the type III PKS family in *D. sinense* [5]. CHS primarily assumes responsibility for catalyzing the stepwise condensation of *p*-coumaric coenzyme A, with three acetate units derived from malonyl coenzyme A, initiating the formation of chalcones [13]. Subsequently, the enzyme chalcone flavanone isomerase (CHI) facilitates the isomerization of chalcone, leading to the formation of flavanone [17]. From these core intermediates, the pathway diverges into various secondary routes, each guiding distinct categories of flavonoids (Figure 1). For instance, dihydroflavonol 4-reductase contributes to flavanols synthesis, flavanone 3-β-hydroxylase to dihydroflavonols, flavonol synthase to flavonols, and anthocianin synthase to anthocyanins [18]. Hence, the sequential condensation step catalyzed by CHS is the rate-limiting process in the biosynthesis of all plant flavonoids.

To systematically identify the type III family of *D. sinense* PKS (DsPKS), the previous data obtained from second- and third-generation sequencing were reanalyzed. The identification of type III DsPKSs was based on conserved domain analysis, followed by phylogenetic classification into distinct clusters. Multiple protein sequence alignments revealed that the *DsCHS3* gene exhibited two alternative splice forms. Prokaryotic expression plasmids of *DsCHS3-1* and *DsCHS3-2* were successfully constructed based on gene cloning techniques. Subsequently, the specific DsCHS3-1 and DsCHS3-2 fusion proteins were purified through GST affinity chromatography. To assess their enzymatic activity, *in vitro* enzyme activity assays were performed utilizing recombinant DsCHS3-1

and DsCHS3-2 proteins. To validate the functional differences in enzyme activity *in vivo*, we conducted complementation experiments by introducing transgenic *DsCHS3-1* and *DsCHS3-2* constructs into *Atchs* (AT5G13930) mutants. This study successfully identified the two alternative splice forms of *DsCHS3* in *D. sinense* and elucidated their distinct activity profiles. These findings provide a foundation for a deeper comprehension of the biosynthetic mechanism underlying flavonoid production.

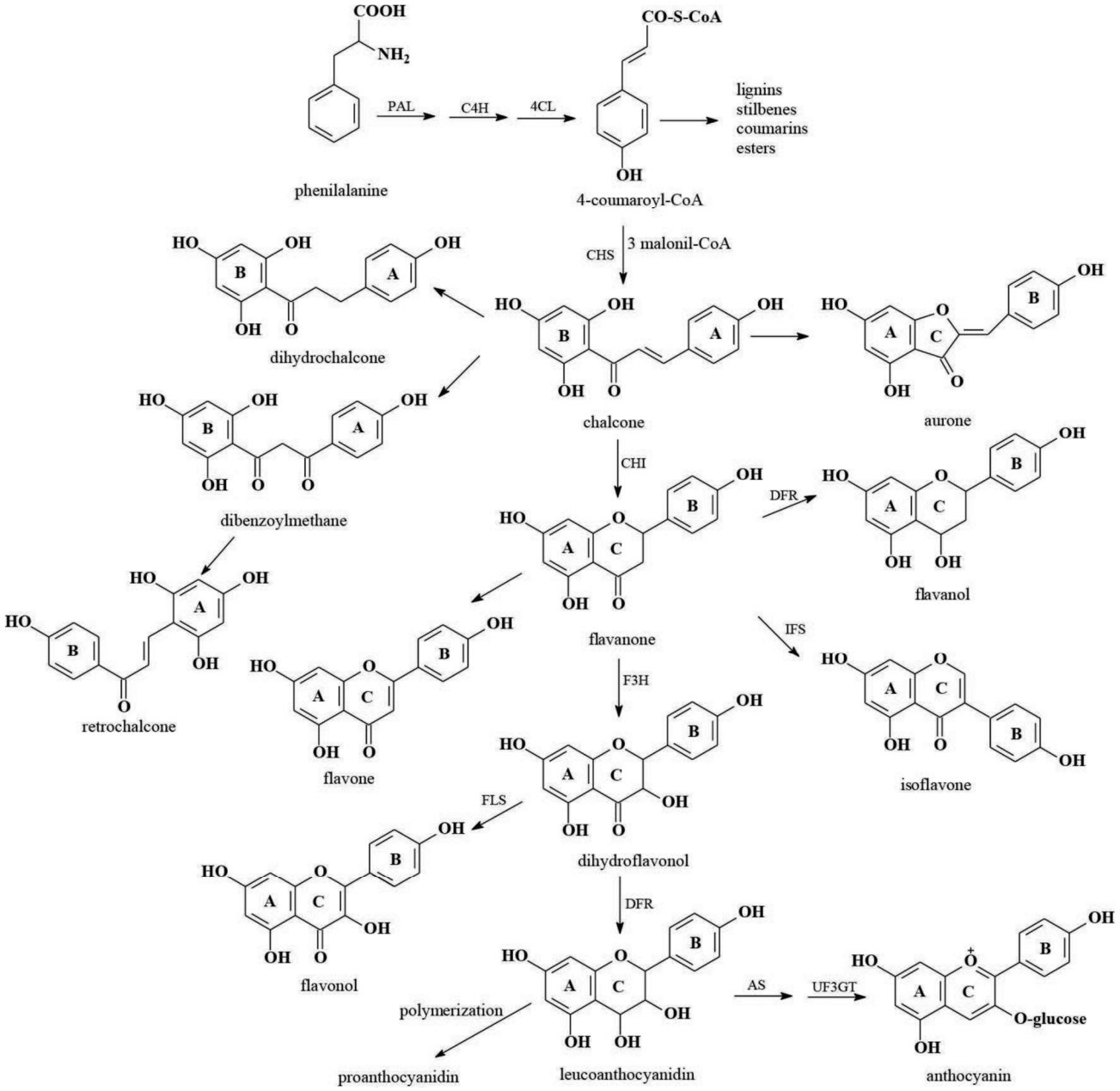

Figure 1. Simplified diagram of the flavonoid biosynthetic pathway. Abbreviations: PAL, phenylalnine amonialyase; C4H, cinnamate 4-hydroxylase; 4CL, 4-coumaroyl-coenzyme A ligase; CHS, chalcone synthase; CHI, chalcone flavanone synthase; F3H, flavanone 3-β-hydroxylase; DFR, dihydroflavonol 4-reductase; FLS, flavonol synthase; IFS, isoflavonoid synthase; AS, anthocianin synthase; UF3GT, UDP glucose: flavonoid 3-O-glucosyltransferase. Cited from Ref. [18].

2. Materials and Methods

2.1. Identification of Type III PKS Genes and Phylogenetic Tree Analysis

The identification of type III *DsPKS* genes in *D. sinense* involved a comprehensive analysis of Illumina and PacBio sequencing data (NCBI BioProject: PRJNA723915) [5,10]. A screening approach was implemented based on the presence of the conserved ketoacyl synthase (KAS) domain within the candidate sequences. Based on the PacBio sequencing data under drought stress [10], the digital expressions of *DsPKS* genes were calculated by Fragments Per Kilobase Million (FPKM) using the TBtools v1.09876 [19].

For comparative analysis, homologous protein sequences of type III PKS from *Arabidopsis thaliana* (AtPKS), *Phalaenopsis equestris* (PePKS), and *Dendrobium catenatum* (DcPKS) were acquired from TAIR10, NCBI ASM126359v1, and NCBI ASM160598v2, respectively. Subsequently, all the protein sequences belonging to the type III PKS family were aligned using ClustalW with default options [20], ensuring the accurate alignment of the conserved regions. To construct a phylogenetic tree, the aligned sequences were processed using MEGA 7.0 software, utilizing the parameters described in the previous study [21].

2.2. Analysis of Conserved Domains

The protein sequences of type III PKSs were compared by Jalview (www.jalview.org/ accessed on 24 July 2023). To validate the alternative splicing types of *DsCHS3-1* and *DsCHS3-2* genes, DNA was extracted from *D. sinense* using a plant tissue DNA extraction kit (Tiangen, Beijing, China). PCR was conducted with primers (AS-F 5′-GCATCTCTCC TTGTCAGTGAT-3′ and AS-R 5′-CGGGTTCTCCTTGAGGATTT-3′) designed to target distinct positions in the *DsCHS3-1* and *DsCHS3-2* genes. Subsequently, the PCR products were sequenced (Sangon, Guangzhou, China) to verify the presence of alternative splicing events.

The three-dimensional structure of the protein was predicted using trRosetta server (yanglab.nankai.edu.cn/trRosetta/help/index.html accessed on 24 July 2023) to observe the difference between DsCHS3-1 and DsCHS3-2 proteins. A homologous 3D model was established using five templates to generate five homologous models, which were sorted based on the TM-score (a confidence score for estimating prediction model quality). The protein's three-dimensional structure was imported into PyMOL 2.5.4 for visualization, and the two structures were superimposed using the align module to compare the differences between the two protein structures.

2.3. Cloning of DsCHS3-1 and DsCHS3-2 Genes

Total RNA was extracted using the RNA Easy Plant Tissue Kit (Taingen, Beijing, China), followed by reverse transcription using the High-Capacity cDNA Archive Kit (Thermo Fisher Scientific, Shanghai, China). The *DsCHS3-1* and *DsCHS3-2* genes were amplified by PCR using cDNA as the template and the following primers: *DsCHS3-1*-F 5′-TCAGTGATAATTAAGAAGGAAACCA-3′ and *DsCHS3-1*-R 5′-CAGCACACTTTATAGTT CCACCC-3′; *DsCHS3-2*-F 5′-CTCAAGGAAAAATTCAAAAGAATGT-3′ and *DsCHS3-2*-R 5′-GCGAGTTGAAGATGAACAGGTAG-3′. The PCR products were cloned into T vectors of PCloneEZ-TOPO (Solarbio, Beijing, China) and sequenced (Sangon, Guangzhou, China).

2.4. Prokaryotic Expression

The *DsCHS3-1* and *DsCHS3-2* genes were both cloned from PCloneEZ-TOPO. Consequently, they share the same forward primer, 5′-GGATAACAATTCCCCTCTAGATGTAAA ACGACGGCCAGT-3′. Both *DsCHS3-1* and *DsCHS3-2* genes have identical 3′ terminal sequences, leading to the utilization of the same reverse primer, 5′-GCAAGCTTGTCGACGGA GCTCTTGGGTACACTGTGGAG-3′. Employing the ClonExpress II One Step Cloning Kit C112-01 (Vazyme, Nanjing, China), the PCR products were integrated into linear pET28a vectors, with double digestion of *Xba*I (BioLabs, Beijng, China) and *Sac*I (BioLabs, Beijng, China), yielding the fusion vectors of *DsCHS3-1*-HisTag and *DsCHS3-2*-HisTag.

Subsequently, the fusion vectors were transferred into competent *Escherichia coli* BL21 (DE3) cells. The bacterial culture was incubated at 37 °C and 180 rpm until the optical den-

sity reached 0.4–0.6. Following this, the recombinant DsCHS-HisTag protein was induced using isopropyl-β-D-thiogalactopyranoside (IPTG) under different conditions to optimize protein solubility. The optimal IPTG concentration was determined by assessing protein solubility at different temperatures, including 23 °C for 16 h, 37 °C for 6 h, and 15 °C for 24 h [22]. According to the selected IPTG concentration and induction temperature, a large-scale bacterial culture was performed. The harvested bacterial solution was centrifuged at 4 °C for 20 min, and the supernatant was carefully decanted. The pellet containing *E. coli* lysate was re-suspended in 150 mL of a 10 mmol/L imidazole solution. Ultrasonication was performed using an ultrasonic instrument on an ice-water mixture for 20 min. The lysate was then centrifuged at 4 °C for 20 min, and the resulting supernatant underwent purification using Ni-IDA resin (Novagen, Madison, WI, USA). The purified protein was analyzed by sodium dodecyl sulfate-polyacrylamide gel electrophoresis (SDS-PAGE) and visualized via Coomassie brilliant blue staining. Additionally, the concentration of the purified protein was determined using a BCA protein concentration detection kit (Bioshorp, Beijing, China).

2.5. Enzyme Activity Assays

For the kinetic analysis, enzymatic reactions were conducted using a reaction mixture consisting of 0.5 mM malonyl-CoA (Yuanye, Shanghai, China), 50 mM Hepes buffer pH 7.0 (Bioshorp, Beijing, China), and 10 μg of the CHS-HisTag fusion protein. The concentration of the *p*-coumaroyl-CoA substrate (Yuanye, Shanghai, China) was varied across the range of 0 to 5 mM (0.0, 0.5, 1.0, 3.0, and 5.0 mM). The reaction volume was adjusted to 50 μL using ddH_2O. The enzymatic reactions were carried out at 37 °C for 30 min, and subsequently terminated by the addition of an equal volume of methanol. Following centrifugation at 12,000 rpm for 10 min, the supernatant was collected and filtered through a 0.22 μm filter membrane. A 20 μL portion of the filtered solution was subjected to analysis by high-performance liquid chromatography (HPLC).

2.6. HPLC Analysis

The samples were detected by LC-100 pump (Wufeng, Shanghai, China) with HC-C18 (18 μm, 4.6 × 250 mm, Agilent, Santa Clara, CA, USA). Chromatographic conditions: column temperature, 30 °C; sample volume, 20 μL, solution A, 0.1% phosphate water; solvent B, 100% acetonitrile; flow rate, 1 mL/min. Setting the mobile phase gradient: 0 min, solution A, 70%, solution B, 30%; 6 min, solution A, 55%, solvent B, 45%; 40 min solution A, 20%, solvent B, 80%. Naringin chalcone (Yuanye, Shanghai, China) was used as the standard substance.

2.7. Eukaryotic Expression

The *DsCHS3-1* and *DsCHS3-2* genes were cloned from PCloneEZ-TOPO and share the same forward (5′-GAGAACACGGGGGACTCTAGATGTAAAACGACGGCCAGT-3′) and reverse (5′-ACGATCGGGAAAATTCGAGCTCCAGGAAACAGCTATGACC-3′) primers. The PCR products were integrated into linear pBI121 vectors (after double digestion of *Xba*I and *Sac*I) using the ClonExpress II One Step Cloning Kit C112-01 (Vazyme, Nanjing, China). The T-DNA insertion mutants of *Atchs* (AT5G13930, SALK_076535C) of Col-0 was bought from AraShare (www.arashare.cn/index/ accessed on 24 July 2023). The homozygotes were screened out using the three-primer method. Transgenic plants were generated using *Agrobacterium tumefaciens* strain EHA105 (WEIDI, Shanghai, China) via the inflorescence dip method [23]. After further kanamycin (Solarbio, Beijing, China) resistance screening and PCR verification, stable genetic lines were obtained.

2.8. Determination of Total Flavonoid Content

A slightly modified version of the previously described sodium nitrite–aluminum nitrate colorimetric method was employed to determine total flavonoids [24]. The flavonoid content in the leaves of one-month-old *Arabidopsis* was detected. A total of 5 g samples

were thoroughly ground and extracted using 50 mL anhydrous ethanol at 90 °C for 2 h. Following centrifugation at 12,000 rpm for 10 min, the supernatant of the extract was transferred to a new centrifuge tube. After rotary evaporation and concentration, 2 mL anhydrous ethanol was mixed, and a 1 mL sample was added into a 25 mL volumetric flask and the volume was fixed with anhydrous ethanol. For each 10 mL sample, 30% anhydrous ethanol was added to 12.5 mL, and 5% sodium nitrite solution was added to 0.75 mL before being shaken and then left to stand for 5 min. Then, 10% aluminum nitrate solution was added to 0.75 mL before being shaken and left to stand for 5 min. Then, 1 mol/L NaOH solution was added to 10 mL, mixed with 30% ethanol volume, and was left to stand for 10 min. Rutin (Yuanye, Shanghai, China) was utilized for generating standard curves. The wavelength of each sample was measured by a spectrophotometer (METASH, Shanghai, China) at 510 nm. The ANOVA analysis ($p < 0.01$) was conducted using SPSS statistical software (version 19).

3. Results

3.1. The Reanalysis of Transcriptome Data to Identify Type III PKSs in D. sinense

To comprehensively investigate the type III *DsPKS* genes in *D. sinense*, the previous transcriptome data downloaded from NCBI BioProject PRJNA723915 were reanalyzed. A total of 10 *DsPKS* genes were identified with the KAS domain. To gain insights into the evolutionary relationships among type III PKS proteins, we constructed a phylogenetic tree using MEGA7.0 software, incorporating type III PKS proteins from *D. sinense*, *D. catenatum*, *Phalaenopsis equestris*, and *A. thaliana*. These proteins were categorized into three distinct groups, namely CHS group, BBS group, and PKS group (Figure 2).

The nomenclature of the 10 *DsPKS* genes was based on a previous investigation of the *DsPKS* family in *D. sinense* [5], along with structural homology comparisons with other PKSs. Among these genes, seven were identified as *DsCHS* genes, two as *DsBBS* genes, and one as a *DsPKS* gene. It is worth noting that, with the exception of *DsCHS1* and *DsCHS4* genes, all other members of the *DsPKS* family exhibited complete open reading frames (ORFs) (Table 1). The lengths of these ORFs ranged from a minimum of 993 nt (DsCHS6), encoding 330 amino acid residues, to a maximum of 1188 nt (DsCHS2 and DsCHS5), encoding 395 amino acid residues (Table 1). Interestingly, the theoretical PI values for all DsPKS proteins were below 7 (Table 1), suggesting an acidic protein nature.

Table 1. Identification of type III *PKS* genes in *D. sinense*.

Names	NCBI ID	Gene ORF			Deduced Polypeptide		
		Start	Stop	Length (nt)	Length (aa)	MW (kDa)	PI
DsCHS1	OP887151	75	>764	-	-	-	-
DsCHS2	OP887152	87	1274	1188	395	43.13	6.22
DsCHS3-1	OP887153	62	1234	1173	390	42.66	5.74
DsCHS3-2	OP887154	22	1017	996	337	36.90	5.43
DsCHS4	OP887155	41	>840	-	-	-	-
DsCHS5	OP887156	36	1223	1188	395	43.19	5.90
DsCHS6	OP887157	108	1100	993	330	35.71	5.62
DsBBS1	OP887149	115	1287	1173	390	42.55	6.28
DsBBS2	OP887150	106	1278	1173	390	42.79	6.03
DsPKS	OP887148	558	1571	1014	337	36.99	5.67

- means an incomplete ORF.

Figure 2. Phylogenetic analysis of type III PKS genes. The protein sequences of type III AtPKS, PePKS, and DcPKS were acquired from TAIR10, NCBI ASM126359v1, and NCBI ASM160598v2, respectively. The TAIR or NCBI accession numbers are given in front of the respective protein name. The phylogenetic tree was preformed using MEGA 7.0 software.

3.2. Conserved Domains in Type III DsPKS Proteins

Based on the results derived from the multiple protein sequence alignment, these type III PKSs collectively share a catalytic core domain characterized by the conserved Cys–His–Asn triad (depicted within the red box in Figure 3a). This pivotal domain orchestrates decarboxylative condensations and cyclization reactions, thereby facilitating the generation of a wide spectrum of PKS products. Additionally, residues believed to play crucial roles in the functional diversity of type III PKSs are identified and highlighted in blue (Figure 3a). It is noteworthy that slight variations in amino acid sequences within the conserved domains

of the DsPKS proteins were discerned (Figure 3a). For instance, in the 202nd position, DsBBS and DsCHS proteins exhibit leucine and threonine, respectively, while in the 274th position, they present alanine and phenylalanine, respectively (Figure 3a). These nuanced alterations within the conserved domain potentially contribute to the functional diversity among the type III DsPKSs.

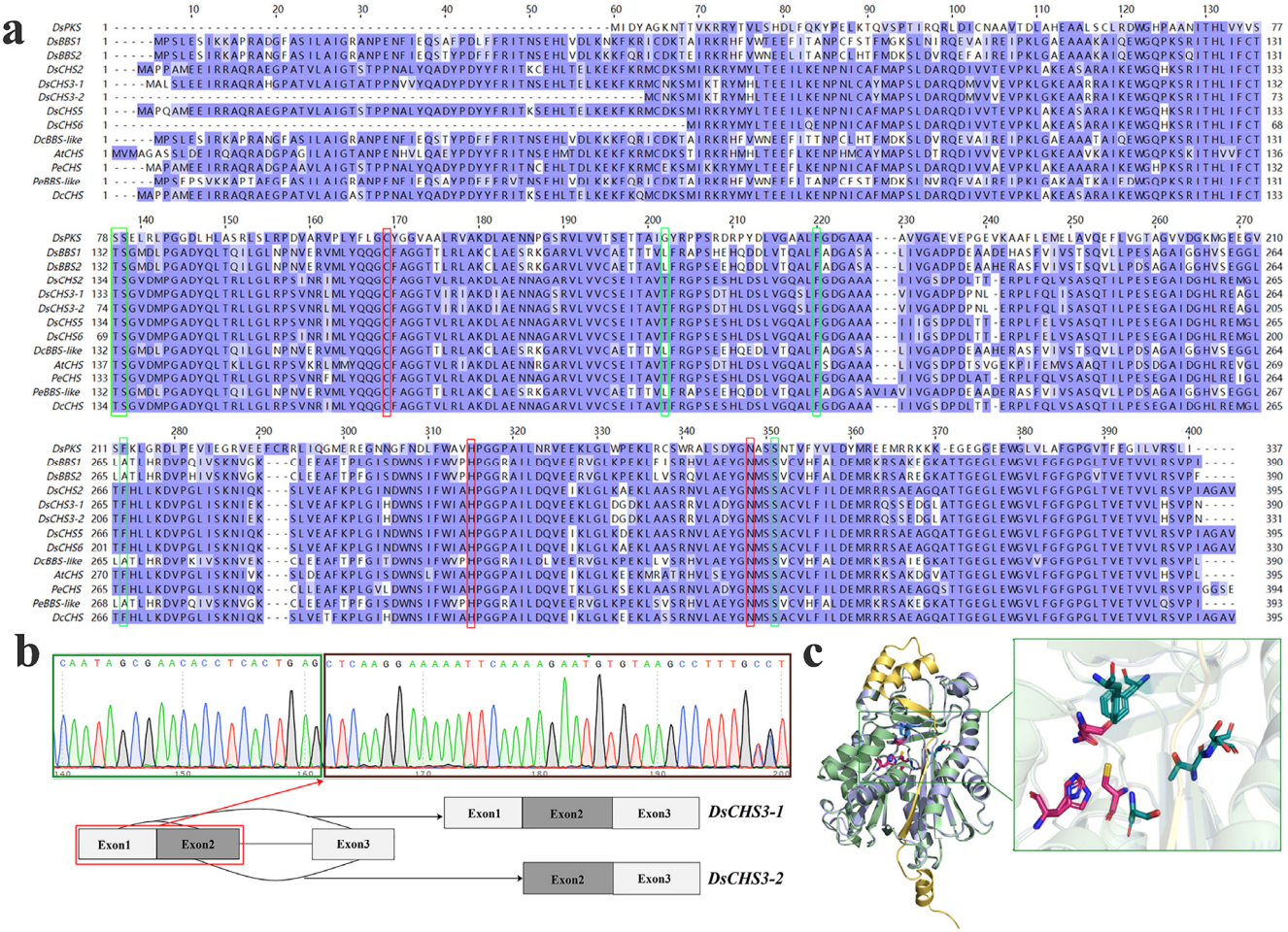

Figure 3. The conservative domain of type III *PKS* genes. (**a**) Sequence alignment of plant type III PKS proteins. The catalytic triad of Cys–His–Asn is highlighted in the red frame. The residues thought to be crucial for the functional diversity of type III PKSs are highlighted in the blue frame (numbering in AtCHS). See Table 1 for detailed accession number information of *D. sinense* proteins. DcBBS-like, XP_020690099.2; AtCHS, AT5G13930.1; PeCHS, AIS35912.1; PeBBS-like, XP_020572025.1; DcCHS, ALE71934.1. (**b**) The two alternative splice forms of the *DsCHS3* gene. Boxes represent exons and introns are represented by black lines between two exons. (**c**) Comparison of three-dimensional structure of DsCHS3-1 and DsCHS3-2 proteins. DsCHS3-1 protein is marked by green, DsCHS3-2 is mar ked by green-blue, and the extra part of DsCHS3-1 protein is marked by yellow.

Intriguingly, the DsCHS3-1 and DsCHS3-2 proteins displayed identical sequences, except for a truncation of 59 amino acid residues at the N-terminus of DsCHS3-2 (Figure 3a). Sequencing analyses confirmed that alternative splicing of the *DsCHS3* gene involved alternative first exons (Figure 3b). To gain further insights into the structural disparities between DsCHS3-1 and DsCHS3-2, homology modeling techniques were employed to predict their three-dimensional structures. The outcome revealed that DsCHS3-1 featured additional secondary structure elements in comparison to DsCHS3-2, specifically three α-helices (Figure 3c, depicted as coils) and two β-sheets (Figure 3c, depicted as arrows). Notably, the two β-sheets of DsCHS3-1 spanned the entrance of the catalytic domain

(Figure 3c). Together, these findings contribute to a deeper understanding of the molecular attributes and functional characteristics of type III DsPKSs in *D. sinense*.

3.3. The Predominant Occurrence of the DsCHS3-1 Splicing Variant in D. sinense

Utilizing the comprehensive full-length transcriptome sequencing data of *D. sinense* under drought stress, the expressions levels of *DsCHS3-1* and *DsCHS3-2* genes were identified. Across all experimental groups, the *DsCHS3-1* expressions significantly outpaced that of *DsCHS3-2* (Figure 4a), indicating that *DsCHS3-1* represents the predominant splicing variant of the *DsCHS3* gene. Intriguingly, under moderate drought conditions, the *DsCHS3-1* expressions showed a decrease compared with the untreated control, while the *DsCHS3-2* expressions remained relatively stable (Figure 4a). However, under severe drought conditions, the expression levels of *DsCHS3-1* were restored to levels similar to those observed in the control, whereas the *DsCHS3-2* expressions decreased (Figure 4a). These findings suggest that the *DsCHS3* gene undergoes distinct alternative splicing patterns in response to different degrees of drought stress.

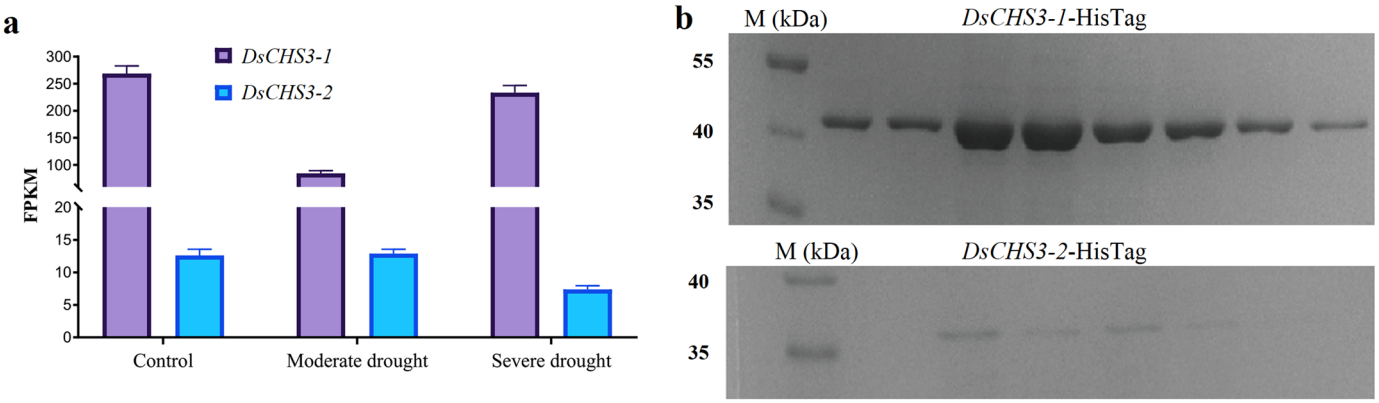

Figure 4. The *DsCHS3-1* and *DsCHS3-2* expressions. (**a**) The expression levels of *DsCHS3-1* and *DsCHS3-2* in *D. sinense* under drought stress. The data were expressed as mean ± standard deviation. (**b**) Purification of recombinant *DsCHS3-1*-HisTag and *DsCHS3-2*-HisTag proteins.

3.4. Prokaryotic Expression of DsCHS3-1 and DsCHS3-2

The *DsCHS3-1* and *DsCHS3-2* were integrated into the pET28a vector, containing a C-terminal hexahistidine tag (HisTag) for affinity chromatography purification. To enhance the yield of high-quality proteins, we conducted an optimization process. Different concentrations of IPTG (0.1, 0.3, 0.5, 0.8, and 1.0 mmol) were utilized to initiate the expression of the recombinant DsCHS-HisTag proteins. The optimal expression of the *DsCHS3-1*-HisTag protein was achieved at 0.5 mmol/L IPTG, while that of the *DsCHS3-2*-HisTag protein occurred at 0.3 mmol/L IPTG (Figure S1). It is worth noting that both recombinant *DsCHS3-1*-HisTag and *DsCHS3-2*-HisTag proteins were predominantly present in the supernatant when cultured at 37 °C (Figure S1). Thus, the conditions of 0.5 mmol/L IPTG at 37 °C and 0.3 mmol/L IPTG at 37 °C are deemed suitable for the expression and subsequent purification of *DsCHS3-1*-HisTag and *DsCHS3-2*-HisTag proteins, respectively.

The purification of *DsCHS3-1*-HisTag and *DsCHS3-2*-HisTag proteins was accomplished using the HisTag affinity purification method. SDS-PAGE analysis of the purified proteins indicated that molecular weights were consistent with their respective theoretical values: *DsCHS3-1* (>40 kDa) and *DsCHS3-2* (>35 kDa) (Figure 4b and Table 1). For the generation of a standard curve, protein standards (bicinchoninic acid reagent) were employed. Based on this curve, the concentration of the purified DsCHS3-1 and DsCHS3-2 proteins was determined. The highest concentration of recombinant DsCHS3-1 and DsCHS3-2 proteins was 0.30 and 0.15 μg/μL, respectively. These meticulously purified protein samples were poised for further comprehensive analyses.

3.5. Enzyme Activity Analysis

To investigate the potential differences in protein kinase activity between the two splice forms of DsCHS3, we performed *in vitro* enzyme characterizations using *p*-coumaroyl-CoA and malonyl-CoA as substrates. HPLC chromatograms were generated to analyze the enzyme assays of *DsCHS3-1* and *DsCHS3-2*, showing a peak aligning with the retention time of the naringin chalcone standard substance (Figure 5a). This finding suggests that both *DsCHS3-1* and *DsCHS3-2* enzymes can catalyze the cyclization and aromatization of *p*-coumarin-CoA and malonyl-CoA, leading to the production of naringin chalcone.

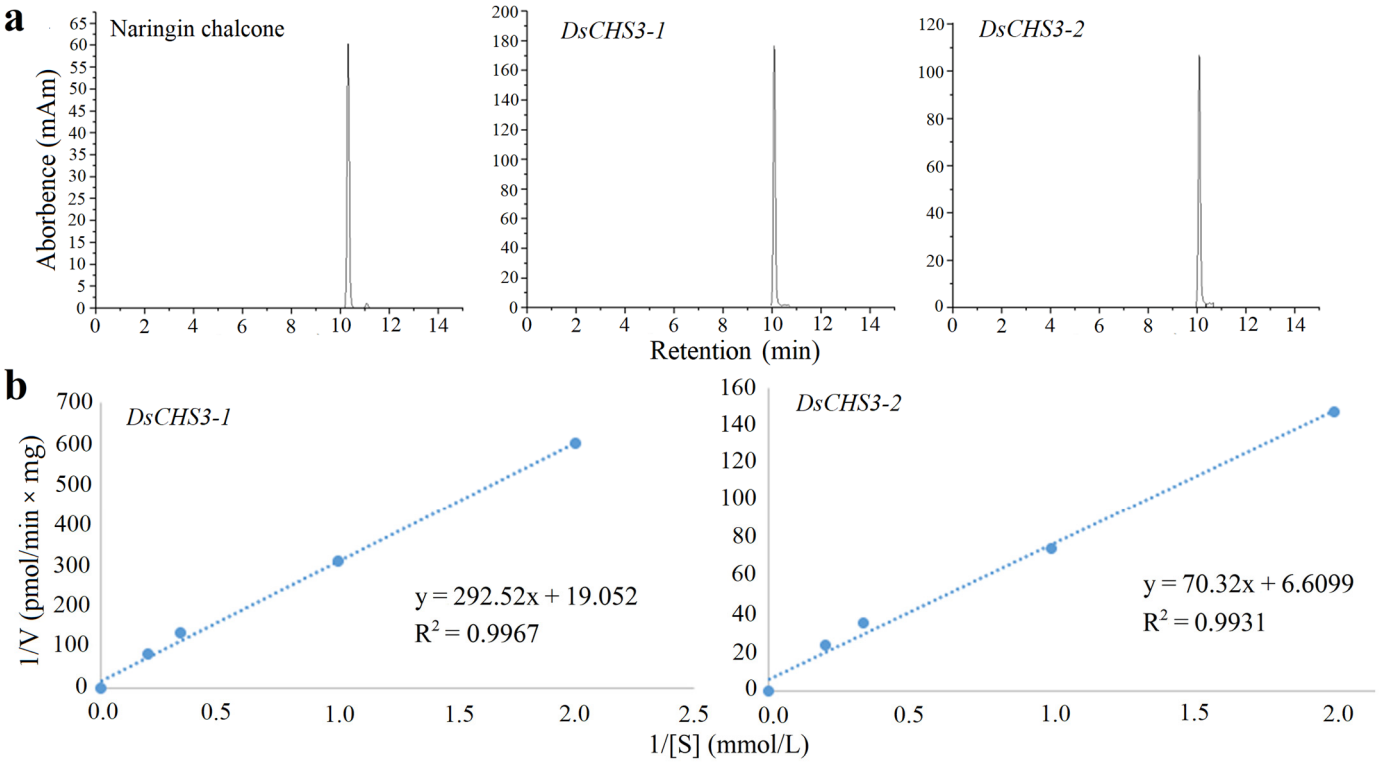

Figure 5. Analysis of *in vitro* enzyme assays. (**a**) HPLC chromatograms of reaction products. Naringin chalcone as standard. (**b**) The Lineweaver–Burk (double reciprocal) plot of *DsCHS3-1* and *DsCHS3-2* enzyme kinetics.

To further assess the catalytic activity of *DsCHS3-1* and *DsCHS3-2* proteins, a statistical analysis of *in vitro* enzyme kinetics was performed by a Lineweaver–Burk (double reciprocal) plot. The outcomes distinctly unveiled noteworthy distinctions between the two splice forms. The Vmax values for chalcone generation were determined as 3.15 pmol/min × mg for *DsCHS3-1* and 9.08 pmol/min × mg for *DsCHS3-2* (Figure 5b). Notably, the Vmax of *DsCHS3-2* was nearly three times higher than that of *DsCHS3-1*, indicating a significantly greater catalytic activity exhibited by *DsCHS3-2*. These findings provide valuable insights into the functional divergence of the two splice forms of *DsCHS3*.

3.6. Functional Complementation Assay

To further explore whether there is a difference in the activity between *DsCHS3-1* and *DsCHS3-2*, it was essential to verify the actual impact of these splice forms on flavonoid biosynthesis *in vivo*. To accomplish this, complementation experiments were conducted using the mutant homozygote (SALK_076535C) of *Atchs* (AT5G13930). The approach of *Agrobacterium*-mediated inflorescence infiltration was employed to generate transgenic *Arabidopsis* plants that expressed *DsCHS3-1* and *DsCHS3-2* within the genetic background of the *Atchs* mutant. By resistance screening and PCR verification, the stable transgenic

Arabidopsis plants were obtained (Figure 6a,b). Three independent transgenic lines were selected for subsequent determination of total flavonoid contents.

To investigate the dynamic changes in flavonoid content, we extracted flavonoids from the leaves of wild-type, mutant, and the *DsCHS3-1* and *DsCHS3-2* complemented lines. Based on the standard curve, the percentage contents were calculated. Notably, the wild-type plants exhibited a flavonoid content of 2.31%, whereas the *Atchs* mutant plants displayed a significantly diminished content of only 0.08% (Figure 6c). This observation clearly indicated that *Atchs* deficiency severely affected flavonoid biosynthesis. Intriguingly, the transgenic complementation lines demonstrated a restoration of flavonoid biosynthesis. The transgenic *DsCHS3-1* complemented lines exhibited a flavonoid content of 1.89%, which closely approached wild-type levels (Figure 6c). Moreover, the transgenic *DsCHS3-2* complemented lines displayed a remarkably higher flavonoid content of 2.85%, surpassing even the levels observed in wild-type plants (Figure 6c). These results strongly suggested that heterologous expression of *DsCHS3-1* and *DsCHS3-2* in *Arabidopsis* successfully compensated for the reduction in flavonoid content caused by the loss of *Atchs* function. Importantly, these results also highlighted the greater *in vivo* catalytic activity of *DsCHS3-2* in comparison to *DsCHS3-1*. These results provide compelling evidence regarding the divergent functional properties of *DsCHS3-1* and *DsCHS3-2* and their influence on flavonoid biosynthesis.

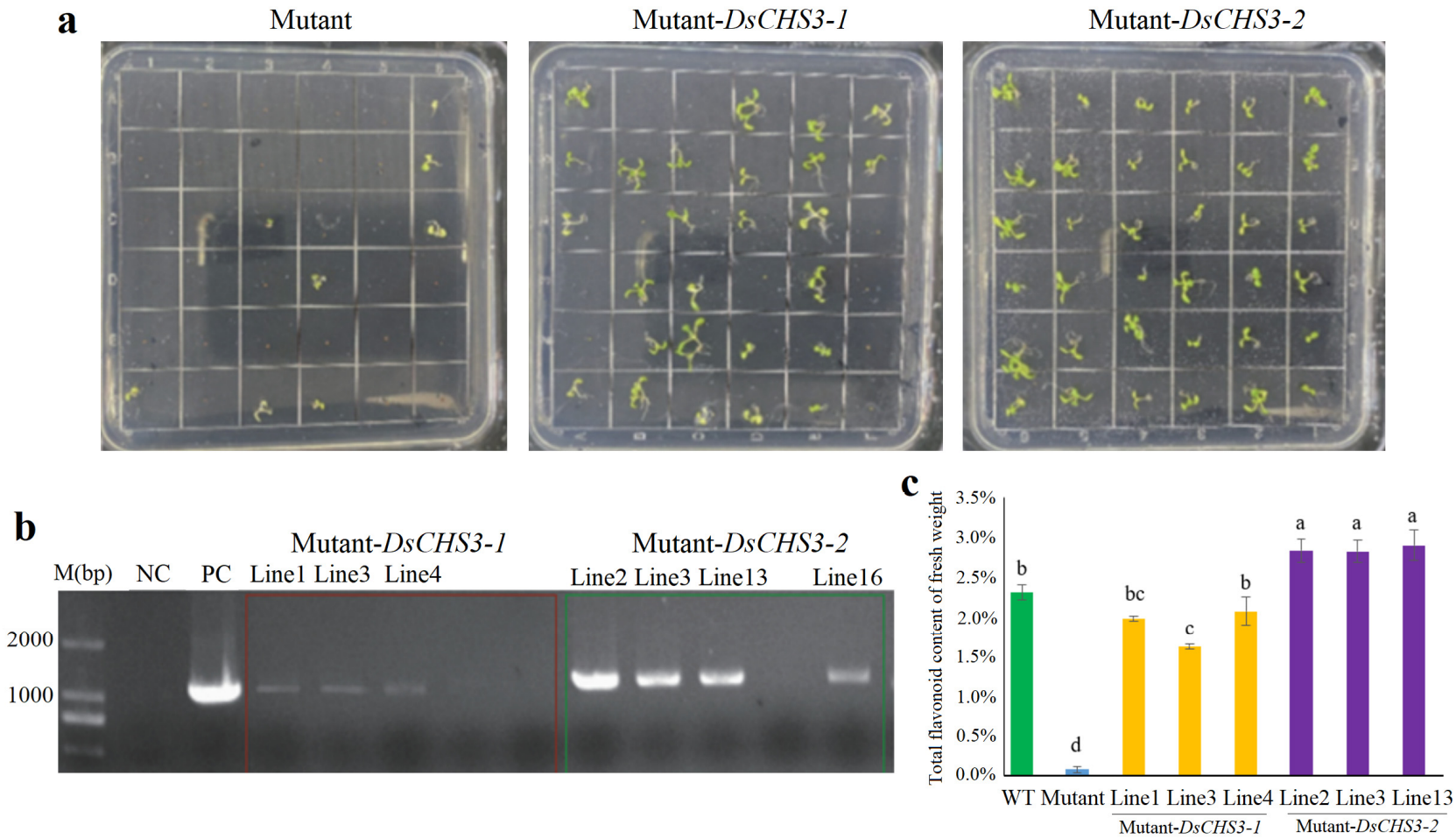

Figure 6. Functional complementation assays in *Arabidopsis thaliana*. (**a**) Transgenic Mutant-*DsCHS3-1* and Mutant-*DsCHS3-2* lines resistance screening. (**b**) Identification of transgenic plants was performed by PCR. NC, negative control; PC, positive control. (**c**) Comparative analysis of total flavonoid contents in different lines. The data were expressed as mean ± standard deviation. The data were compared by Duncan Multiple test. Different lowercase letters represent significant differences, and the same lowercase letters represent no significant differences ($p < 0.01$).

4. Discussion

Dendrobium sinense, a native orchid species in China, is gaining increasing attention due to its remarkable aesthetic appeal and valuable medicinal properties [5,7]. This species has been recognized as a traditional Chinese herbal medicine, revered for its antioxidant, antibacterial, and antitumor capabilities, which can be attributed to the presence of various bioactive compounds, including alkaloids, flavonoids, and bibenzyls [6,9]. Despite its significance, limited research has been conducted on the regulatory mechanisms underlying the biosynthesis of these bioactive compounds in *D. sinense*. Our previously comprehensive transcriptomic analysis offers a significant opportunity to elucidate the intricate secondary metabolic processes occurring in *D. sinense* and serves as a valuable resource for exploring gene families associated with these processes [5,10].

Polyketides, a class of biologically active natural products in plants, are synthesized through the condensation of acyl-thioester units, such as malonyl-CoA and methylmalonyl-CoA, resulting in the formation of metabolites with a wide range of structures and biological activities [14]. Plant type III PKSs have been widely studied since their initial discovery in parsley [25], and they play a crucial role in the biosynthesis of various plant metabolites [11]. Utilizing the comprehensive transcriptome data obtained from previous studies [5,10], a total of 10 type III *DsPKS* genes were successfully identified in *D. sinense*. The incorporation of multiple transcriptome data sources in this study has led to the identification of a greater number of type III *DsPKS* genes compared to the previous report [5]. These lengths of type III DsPKS proteins were consistent with a previous report that plant type III PKSs consist of approximately 400 amino acid [11].

Despite the existence of over 20 different members of plant type III PKSs with diverse functions [12], the type III PKS proteins from *D. sinense* were classified into three distinct groups, namely CHS group, BBS group, and PKS group. Notably, the PKS group comprised the largest number of members among the identified type III PKS proteins in *D. sinense*. This classification highlights the diversity and functional specialization within the type III PKS family in *D. sinense*, further emphasizing the importance of these enzymes in the synthesis of various metabolites in this orchid species. Future investigations into the specific functions and regulatory mechanisms of these type III PKS genes in *D. sinense* will provide valuable insights into the biosynthesis of bioactive compounds in this plant species and broaden our understanding of the unique metabolic pathways present in orchids.

CHS is a member of the type III PKS family, responsible for catalyzing the condensation reaction between one molecule of *p*-coumaroyl-CoA and three molecules of malonyl-CoA. This enzymatic reaction leads to the formation of naringenin chalcone, which serves as a key precursor for the biosynthesis of a wide range of flavonoids, including flavones, flavonols, flavanones, and anthocyanins (Figure 1) [12]. The overall three-dimensional fold of plant type III PKSs is highly conserved, characterized by a catalytic core domain composed of the Cys–His–Asn triad [26]. This conserved triad, depicted by a red box in Figure 3a, plays a crucial role in decarboxylative condensation and cyclization reactions that give rise to the diverse array of products produced by PKS enzymes [13]. Recent crystallographic and site-directed studies revealed that even small modification in the active site architecture can result in the functional diversity of the type III PKSs [27]. In *D. sinense*, the DsBBS and DsCHS proteins were found to possess specific amino acid residues at positions 202 (leucine and threonine) and 274 (alanine and phenylalanine), respectively (Figure 3a). Our previous *in vitro* enzyme assay confirmed that the DsBBS1 protein could catalyze the cyclization and aromatization of *p*-coumaryol-CoA and malonyl-CoA to generate bibenzyls [5]. In the present study, we have identified *DsCHS3* proteins as being involved in chalcone biosynthesis, further highlighting the functional diversity within the type III DsPKS family. It is plausible that these small modifications within the conserved domain contribute to the generation of functional diversity among type III DsPKS enzymes. To elucidate the relationship between amino acid residue changes and catalytic activity in type III PKS enzymes, additional investigations are warranted. Future

studies could involve site-directed mutagenesis to introduce specific amino acid changes at key positions and subsequently assess the impact on catalytic efficiency.

Interestingly, upon conducting multiple sequence alignment, it was observed that the gene sequences of *DsCHS3-1* and *DsCHS3-2* were identical, except for a notable difference at the 5′ end, where the *DsCHS3-1* gene exhibited an additional 217-base segment. Thus, the full-length transcripts suggested the presence of alternative splice forms of the *DsCHS3* gene. Alternative splicing is a widespread process in cellular gene expression, where different combinations of exons within a pre-mRNA are selectively joined, giving rise to multiple mRNA isoforms [28]. This dynamic mechanism substantially enhances proteomic diversity by generating distinct protein variants with unique functions or regulatory properties [29]. Various types of alternative splicing events have been characterized, including intron retention, exon skipping, mutually exclusive exons, alternative 5′ or 3′ splicing sites, alternative first exons, and alternative last exons [30,31]. Although intron retention is the most prevalent form of alternative splicing in plants [31], the alternative splicing of *DsCHS3* exhibited two distinct alternative first exons, as determined by Sanger sequencing. Based on the systematic analysis of alternative first exons in plants, the alternative splicing pattern observed in *DsCHS3* can be classified as type II of alternative first exons, where the first exon of one gene structure serves as an internal exon within an alternative gene structure [32]. Usually, different promoters can initiate transcription at the beginning of a gene, particularly when multiple transcription start sites are present, leading to the inclusion of different first exons [33]. Additionally, specific transcription factors are known to exert influence over the selection of alternative first exons [32]. Further investigations are warranted to elucidate the underlying mechanisms governing the generation of alternative first exons in *DsCHS3*, including the identification of regulatory elements, transcription factors, or other factors that contribute to the selection and usage of specific first exons.

Alternative splicing is a widespread phenomenon in plants, playing a critical role in the regulation of gene expression and protein diversity across various biological processes, including development, tissue-specific gene expression, and environmental responses [30,34]. Importantly, alternative splicing has emerged as a key regulatory mechanism governing secondary metabolism [31,35]. Advancements in third-generation sequencing technology have revealed that alternative splicing contributes to the regulation of genes involved in flavonoid biosynthesis and their transcriptional regulators [36–38]. Despite systematic investigations of alternative first exons being conducted in model plants of *Oryza sativa* and *A. thaliana* [32,39], our understanding of alternative first exons in *D. sinense* remains limited. Through full-length transcriptome sequencing, the *DsCHS3* gene underwent different alternative splicing patterns, and *DsCHS3-1* was characterized as the main product of alternative splicing. Moreover, the expression profiles of *DsCHS3-1* and *DsCHS3-2* were tightly regulated in response to varying degrees of drought stress, suggesting a potential role for the alternative first exons of *DsCHS3* in the plant's response to drought stress. It is plausible that different promoters and transcription factors associated with *DsCHS3-1* and *DsCHS3-2* may confer an additional layer of gene expression regulation [39]. Elucidating the regulatory impact of alternative splicing on CHS activity holds significant importance as it can provide valuable insights into flavonoid biosynthesis and their functions in plant physiology and defense responses. In plants, CHS catalyzes the initial and rate-limiting step in flavonoid biosynthesis, thereby controlling the flow of substrates into the flavonoid pathway [12]. Flavonoids are multifunctional compounds that play crucial roles in plant growth, development, defense against stresses, and plant-microbe interactions [40]. Thus, alternative splicing serves as a regulatory mechanism to fine-tune CHS activity, which may be crucial for the control of flavonoid biosynthesis in response to drought stress.

The utilization of alternative first exons in gene transcription can result in the generation of alternative transcription start sites (ATGs), thereby giving rise to protein variants with distinct N-termini. This diversity in N-terminal sequences has been demonstrated to contribute to functional differences among protein isoforms [41]. Interestingly, three-dimensional structure analysis revealed that the DsCHS3-1 protein possesses additional

α-helices and β-sheets at the N-terminus compared to the DsCHS3-2 protein. Notably, these two extra β-sheets are positioned adjacent to the catalytic structural domain of the DsCHS3-1 protein. Consequently, it is conceivable that the unique structural characteristics of the DsCHS3-1 protein may impact its catalytic activity. To further investigate the functional implications of these structural differences, *in vitro* enzyme assays were performed. Surprisingly, the *in vitro* enzyme assay indicated that the catalytic efficiency of DsCHS3-2 activity was three times higher than that of the DsCHS3-1 activity. In addition, in-depth functional analyses were conducted through transgenic complementation tests *in vivo*, which corroborated the findings from the enzyme assays. These tests demonstrated that the DsCHS3-2 protein exhibited higher catalytic activity. The comprehensive evaluation of enzyme activity both *in vitro* and *in vivo* strongly supports the notion that the alternative first exons can regulate the functional properties of the DsCHS3 proteins, as previously reported in related studies [41,42]. The observed structural differences between the DsCHS3-1 and DsCHS3-2 proteins, particularly in their N-terminal regions, suggest that alternative splicing can modulate the conformation and activity of the resulting protein isoforms. The presence of additional α-helices and β-sheets in the N-terminus of DsCHS3-1 may influence its interactions with substrates, cofactors, or regulatory molecules, potentially leading to altered enzymatic activity. Further investigations into the precise molecular mechanisms underlying these functional disparities are warranted to gain a deeper understanding of how alternative splicing modulates the activity and regulation of *DsCHS3* isoforms.

5. Conclusions

Transcriptome data revealed the presence of 10 *DsPKS* genes with the KAS domain, which were categorized into three groups: CHS group, BBS group, and PKS group. The characterization of type III *DsPKS* genes contributes to a comprehensive understanding of the secondary metabolite synthesis in *D. sinense*. Alternative splicing of the *DsCHS3* gene was observed, resulting in the generation of two splice forms, *DsCHS3-1* and *DsCHS3-2*. Full-length cDNA sequencing revealed that *DsCHS3-1* was the predominant splice variant. Enzyme activity analysis indicated that DsCHS3-2 exhibited significantly higher catalytic activity compared to DsCHS3-1. Functional complementation assays in *Arabidopsis* confirmed that both *DsCHS3-1* and *DsCHS3-2* were able to restore flavonoid biosynthesis in the *Atchs* mutant, indicating their functional similarity. However, *DsCHS3-2* showed a more pronounced effect, leading to a higher flavonoid content compared to wild-type plants. These findings suggest that the alternative first exons in the *DsCHS3* gene influence DsCHS3-1 and DsCHS3-2 enzyme activity.

Supplementary Materials: The following supporting information can be downloaded at: https://www.mdpi.com/article/10.3390/f14091702/s1, Figure S1: Optimization of induction conditions for soluble expression of *DsCHS3-1*-HisTag and *DsCHS3-2*-HisTag proteins. (a) Different IPTG concentrations induce recombinant protein. (b) Induction of recombinant proteins at the same IPTG concentration at different temperatures and times.

Author Contributions: Y.W., conceptualization, investigation, and writing—original draft; L.L., writing—original draft, investigation, and formal analysis; Q.O., validation and resources; H.Y., visualization and validation; J.W., funding acquisition, project administration, and supervision; J.N., funding acquisition, methodology, and writing—review and editing. All authors have read and agreed to the published version of the manuscript.

Funding: This work was supported by Hainan Provincial Natural Science Foundation of China (320RC469), Collaborative Innovation Center Project of Hainan University (XTCX2022STC03), and Hainan University Research Project (KYQD(ZR)-22056).

Data Availability Statement: Authors can confirm that all relevant data are included in the paper and/or its supplementary information files.

Conflicts of Interest: The authors declare no conflict of interest.

References

1. Chase, M.W.; Cameron, K.M.; Freudenstein, J.V.; Pridgeon, A.M.; Salazar, G.; Van den Berg, C.; Schuiteman, A. An updated classification of Orchidaceae. *Bot. J. Linn. Soc.* **2015**, *177*, 151–174. [CrossRef]
2. Zotz, G.; Bader, M. Epiphytic plants in a changing world-global: Change effects on vascular and non-vascular epiphytes. In *Progress in Botany*; Springer: Berlin/Heidelberg, Germany, 2009; pp. 147–170.
3. He, L.; Su, Q.; Bai, L.; Li, M.; Liu, J.; Liu, X.; Zhang, C.; Jiang, Z.; He, J.; Shi, J. Recent research progress on natural small molecule bibenzyls and its derivatives in *Dendrobium* species. *EUR. J. Med. Chem.* **2020**, *204*, 112530. [CrossRef] [PubMed]
4. Pan, L.-H.; Li, X.-F.; Wang, M.-N.; Zha, X.-Q.; Yang, X.-F.; Liu, Z.-J.; Luo, Y.-B.; Luo, J.-P. Comparison of hypoglycemic and antioxidative effects of polysaccharides from four different *Dendrobium* species. *Int. J. Biol. Macromol.* **2014**, *64*, 420–427. [CrossRef] [PubMed]
5. Chen, Y.; Wang, Y.; Liang, C.; Liu, L.; Song, X.; Zhao, Y.; Wang, J.; Niu, J. Characterization of the Key Bibenzyl Synthase in *Dendrobium sinense*. *Int. J. Mol. Sci.* **2022**, *23*, 6780. [CrossRef]
6. Chen, X.-J.; Mei, W.-L.; Zuo, W.-J.; Zeng, Y.-B.; Guo, Z.-K.; Song, X.-Q.; Dai, H.-F. A new antibacterial phenanthrenequinone from *Dendrobium sinense*. *J. Asian Nat. Prod. Res.* **2013**, *15*, 67–70. [CrossRef]
7. Cai, C.-H.; Tan, C.-Y.; Chen, H.-Q.; Wang, H.; Mei, W.-L.; Song, X.-Q.; Dai, H.-F. Chemical constituents from *Dendrobium sinense* (II). *Guihaia* **2020**, *40*, 1368–1374. [CrossRef]
8. Tan, C.-Y.; Mei, W.-L.; Zhao, Y.-X.; Huang, S.-Z.; Kong, F.-D.; Yang, N.-N.; Song, X.-Q.; Dai, H.-F. Chemical Constituents from *Dendrobium sinense*. *J. Trop. Subtrop. Bot.* **2017**, *25*, 189. [CrossRef]
9. Chen, X.-J.; Mei, W.-L.; Cai, C.-H.; Guo, Z.-K.; Song, X.-Q.; Dai, H.-F. Four new bibenzyl derivatives from *Dendrobium sinense*. *Phytochem. Lett.* **2014**, *9*, 107–112. [CrossRef]
10. Zhang, C.; Chen, J.; Huang, W.; Song, X.; Niu, J. Transcriptomics and metabolomics reveal purine and phenylpropanoid metabolism response to drought stress in *Dendrobium sinense*, an endemic orchid species in Hainan Island. *Front. Genet.* **2021**, *12*, 1039. [CrossRef]
11. Yu, D.; Xu, F.; Zeng, J.; Zhan, J. Type III polyketide synthases in natural product biosynthesis. *IUBMB Life* **2012**, *64*, 285–295. [CrossRef]
12. Shimizu, Y.; Ogata, H.; Goto, S. Type III polyketide synthases: Functional classification and phylogenomics. *ChemBioChem* **2017**, *18*, 50–65. [CrossRef] [PubMed]
13. Abe, I. Biosynthesis of medicinally important plant metabolites by unusual type III polyketide synthases. *J. Nat. Med.* **2020**, *74*, 639–646. [CrossRef]
14. Lin, Z.; Qu, X. Emerging Diversity in Polyketide Synthase. *Tetrahedron Lett.* **2022**, *110*, 154183. [CrossRef]
15. Flores-Sanchez, I.J.; Verpoorte, R. Plant polyketide synthases: A fascinating group of enzymes. *Plant Physiol. Bioch.* **2009**, *47*, 167–174. [CrossRef] [PubMed]
16. Tsai, S.-C. The structural enzymology of iterative aromatic polyketide synthases: A critical comparison with fatty acid synthases. *Annu. Rev. Biochem.* **2018**, *87*, 503–531. [CrossRef] [PubMed]
17. Shui, L.; Huo, K.; Chen, Y.; Zhang, Z.; Li, Y.; Niu, J. Integrated metabolome and transcriptome revealed the flavonoid biosynthetic pathway in developing *Vernonia amygdalina* leaves. *PeerJ* **2021**, *9*, e11239. [CrossRef] [PubMed]
18. Santos, E.L.; Maia, B.; Ferriani, A.P.; Teixeira, S.D. Flavonoids: Classification, biosynthesis and chemical ecology. In *Flavonoids—From Biosynthesis to Human Health*; InTechOpen: London, UK, 2017; Volume 13, pp. 78–94.
19. Chen, C.; Chen, H.; Zhang, Y.; Thomas, H.R.; Frank, M.H.; He, Y.; Xia, R. TBtools: An integrative toolkit developed for interactive analyses of big biological data. *Mol. Plant* **2020**, *13*, 1194–1202. [CrossRef]
20. Thompson, J.D.; Higgins, D.G.; Gibson, T.J. CLUSTAL W: Improving the sensitivity of progressive multiple sequence alignment through sequence weighting, position-specific gap penalties and weight matrix choice. *Nucleic Acids Res.* **1994**, *22*, 4673–4680. [CrossRef]
21. Niu, J.; Bi, Q.; Deng, S.; Chen, H.; Yu, H.; Wang, L.; Lin, S. Identification of *AUXIN RESPONSE FACTOR* gene family from *Prunus sibirica* and its expression analysis during mesocarp and kernel development. *BMC Plant Biol.* **2018**, *18*, 21. [CrossRef]
22. Porowińska, D.; Wujak, M.; Roszek, K.; Komoszyński, M. Prokaryotic expression systems. *Adv. Hyg. Exp. Med.* **2013**, *67*, 119–129. [CrossRef]
23. Zhang, X.; Henriques, R.; Lin, S.-S.; Niu, Q.-W.; Chua, N.-H. *Agrobacterium*-mediated transformation of *Arabidopsis thaliana* using the floral dip method. *Nat. Protoc.* **2006**, *1*, 641–646. [CrossRef] [PubMed]
24. Liu, X.-m.; Liu, Y.; Shan, C.-h.; Yang, X.-q.; Zhang, Q.; Xu, N.; Xu, L.-y.; Song, W. Effects of five extraction methods on total content, composition, and stability of flavonoids in jujube. *Food Chem. X* **2022**, *14*, 100287. [CrossRef] [PubMed]
25. Reimold, U.; Kröger, M.; Kreuzaler, F.; Hahlbrock, K. Coding and 3′ non-coding nucleotide sequence of chalcone synthase mRNA and assignment of amino acid sequence of the enzyme. *EMBO J.* **1983**, *2*, 1801–1805. [CrossRef]
26. Lim, Y.P.; Go, M.K.; Yew, W.S. Exploiting the biosynthetic potential of type III polyketide synthases. *Molecules* **2016**, *21*, 806. [CrossRef] [PubMed]
27. Morita, H.; Wong, C.P.; Abe, I. How structural subtleties lead to molecular diversity for the type III polyketide synthases. *J. Biol. Chem.* **2019**, *294*, 15121–15136. [CrossRef] [PubMed]
28. Mazin, P.V.; Khaitovich, P.; Cardoso-Moreira, M.; Kaessmann, H. Alternative splicing during mammalian organ development. *Nat. Genet.* **2021**, *53*, 925–934. [CrossRef]

29. Ule, J.; Blencowe, B.J. Alternative splicing regulatory networks: Functions, mechanisms, and evolution. *Mol. Cell* **2019**, *76*, 329. [CrossRef]
30. Syed, N.H.; Kalyna, M.; Marquez, Y.; Barta, A.; Brown, J.W. Alternative splicing in plants–coming of age. *Trends Plant Sci.* **2012**, *17*, 616. [CrossRef]
31. Lam, P.Y.; Wang, L.; Lo, C.; Zhu, F.-Y. Alternative splicing and its roles in plant metabolism. *Int. J. Mol. Sci.* **2022**, *23*, 7355. [CrossRef]
32. Chen, W.-H.; Lv, G.; Lv, C.; Zeng, C.; Hu, S. Systematic analysis of alternative first exons in plant genomes. *BMC Plant Biol.* **2007**, *7*, 55. [CrossRef]
33. Turner, J.D.; Schote, A.B.; Macedo, J.A.; Pelascini, L.P.; Muller, C.P. Tissue specific glucocorticoid receptor expression, a role for alternative first exon usage? *Biochem. Pharmacol.* **2006**, *72*, 1529–1537. [CrossRef]
34. He, B.; Han, X.; Liu, H.; Bu, M.; Cui, P.; Xu, L.-A. Deciphering alternative splicing patterns in multiple tissues of *Ginkgo biloba* important secondary metabolites. *Ind. Crop. Prod.* **2022**, *181*, 114812. [CrossRef]
35. Qiao, D.; Yang, C.; Chen, J.; Guo, Y.; Li, Y.; Niu, S.; Cao, K.; Chen, Z. Comprehensive identification of the full-length transcripts and alternative splicing related to the secondary metabolism pathways in the tea plant (*Camellia sinensis*). *Sci. Rep.* **2019**, *9*, 2709. [CrossRef]
36. Deng, Y.; Lu, S. Biosynthesis and regulation of phenylpropanoids in plants. *Crit. Rev. Plant Sci.* **2017**, *36*, 257–290. [CrossRef]
37. Tang, W.; Zheng, Y.; Dong, J.; Yu, J.; Yue, J.; Liu, F.; Guo, X.; Huang, S.; Wisniewski, M.; Sun, J. Comprehensive transcriptome profiling reveals long noncoding RNA expression and alternative splicing regulation during fruit development and ripening in kiwifruit (*Actinidia chinensis*). *Front. Plant Sci.* **2016**, *7*, 335. [CrossRef]
38. Ye, J.; Cheng, S.; Zhou, X.; Chen, Z.; Kim, S.U.; Tan, J.; Zheng, J.; Xu, F.; Zhang, W.; Liao, Y. A global survey of full-length transcriptome of Ginkgo biloba reveals transcript variants involved in flavonoid biosynthesis. *Ind. Crop. Prod.* **2019**, *139*, 111547. [CrossRef]
39. Kitagawa, N.; Washio, T.; Kosugi, S.; Yamashita, T.; Higashi, K.; Yanagawa, H.; Higo, K.; Satoh, K.; Ohtomo, Y.; Sunako, T. Computational analysis suggests that alternative first exons are involved in tissue-specific transcription in rice (*Oryza sativa*). *Bioinformatics* **2005**, *21*, 1758–1763. [CrossRef] [PubMed]
40. Ferreyra, M.L.F.; Serra, P.; Casati, P. Recent advances on the roles of flavonoids as plant protective molecules after UV and high light exposure. *Physiol. Plant.* **2021**, *173*, 736–749. [CrossRef] [PubMed]
41. Ouelle, D.E.; Zindy, F.; Ashmun, R.A.; Sherr, C.J. Alternative reading frames of the INK4a tumor suppressor gene encode two unrelated proteins capable of inducing cell cycle arrest. *Cell* **1995**, *83*, 993–1000. [CrossRef] [PubMed]
42. Maniatis, T.; Tasic, B. Alternative pre-mRNA splicing and proteome expansion in metazoans. *Nature* **2002**, *418*, 236–243. [CrossRef] [PubMed]

Disclaimer/Publisher's Note: The statements, opinions and data contained in all publications are solely those of the individual author(s) and contributor(s) and not of MDPI and/or the editor(s). MDPI and/or the editor(s) disclaim responsibility for any injury to people or property resulting from any ideas, methods, instructions or products referred to in the content.